Hindawi
International Journal of Chemical Engineering
Volume 2022, Article ID 8303874, 14 pages
https://doi.org/10.1155/2022/8303874

Research Article

Reaction Kinetics of Cinnamaldehyde Hydrogenation over Pt/SiO_2: Comparison between Bulk and Intraparticle Diffusion Models

Ali Al-Shathr,[1] Zaidoon M. Shakor,[1] Bashir Y. Al-Zaidi,[1] Hasan Sh. Majdi,[2] Adnan A. AbdulRazak,[1] Safa Aal-Kaeb,[1] Adel A. Shohib,[3] and James McGregor[4]

[1]*Chemical Engineering Department, University of Technology-Iraq, Baghdad 10066, Iraq*
[2]*Chemical Engineering and Oil Refinery Department, AlMustaqbal University College, Hilla, Babylon, Iraq*
[3]*Engineering College, Misan University, Misan, Iraq*
[4]*University of Sheffield, Department of Chemical and Biological Engineering, Mappin Street, Sheffield S1 3JD, UK*

Correspondence should be addressed to Adnan A. AbdulRazak; adnansss2002@yahoo.com

Received 17 December 2021; Revised 7 April 2022; Accepted 20 June 2022; Published 7 July 2022

Academic Editor: Prem Kumar Seelam

The liquid-phase hydrogenation of cinnamaldehyde over a Pt/SiO_2 catalyst was investigated experimentally and theoretically. The experiments were conducted in a 300 cm^3 stainless steel stirred batch reactor supplied with hydrogen gas and ethanol as a solvent. Five Langmuir–Hinshelwood kinetic models were investigated to fit the experimental data. The predictions from the bulk model were compared with predictions from the intraparticle diffusion model. Competitive and non-competitive mechanisms were applied to produce the main intermediate compound, cinnamyl alcohol. Reaction rate parameters for the different reaction steps were calculated by comparing between the experimental and mathematical models. All rate data utilized in the present study were obtained in the kinetic regime. The kinetic parameters were obtained by applying a nonlinear dynamic optimization algorithm. Nevertheless, the comparison between the methodology of the present model and these five models indicated that the non-competitive mechanism is more acceptable and identical with the single-site Langmuir–Hinshelwood kinetic model including mass transfer effects and it mimicked the reactant behavior better than the other models. In addition, the observed mean absolute error (MAE) for the non-competitive mechanism of the present model was 2.3022 mol/m^3; however, the MAE for the competitive mechanism was 2.8233 mol/m^3, which is an increase of approximately 18%. The prediction of the intraparticle diffusion model was found to be very close to that of the bulk model owing to the use of a catalyst with a very small particle size (<40 microns). Employing a commercial 5% Pt/SiO_2 catalyst showed a result consistent with previous research using different catalysts, with an activation energy of ≈24 kJ/mol.

1. Introduction

During recent decades, increasing global population has fueled demand for energy vectors, and commodity, specialty, and fine chemicals. One important group of chemicals which has seen such growth in demand is α, β-unsaturated aldehydes. This has forced a reevaluation of the current methods used to produce these substances [1–3]. Of particular note is cinnamaldehyde (CALD), the hydrogenation of which in the liquid phase generates valuable chemicals through consecutive reactions [4]. This reaction provides an excellent opportunity to study the influence of catalyst and operating conditions on the reactant conversion and selectivity in molecules containing multiple reactive functionalities and serves as an exemplar molecular for other α, β-unsaturated aldehydes and ketones.

Cinnamaldehyde consists of conjugated C=C and C=O bonds connected to an aromatic ring [1, 5, 6]. Borovinskaya [7] and Chang et al. [4] studied the reaction pathway of the direct hydrogenation of cinnamaldehyde to hydrocinnamyl alcohol; however, other researchers have identified two indirect pathways via cinnamyl alcohol of hydrocinnamaldehyde, as shown in Figure 1 [1, 2, 5, 8–24].

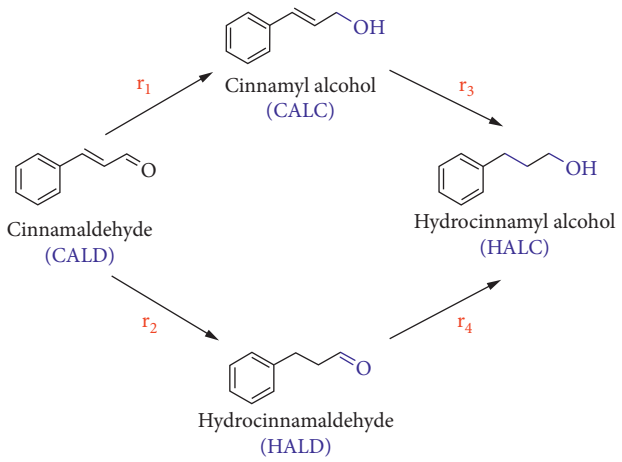

Figure 1: Reaction scheme of cinnamaldehyde hydrogenation.

Of the three possible hydrogenation products, cinnamyl alcohol is the most favored as it has a wide variety of applications, including as a flavor in bakery goods, confectionary, and beverages; as an animal or flea repellent; as protection for plants against nematodes; as an antimicrobial agent; as a component of air fresheners; and in the medical field [4, 25]. In general, C=C hydrogenation is thermodynamically favored whereas alcohol desorption is slower which means that hydrocinnamaldehyde is often the main product. In this reaction, the production of cinnamyl alcohol as an intermediary compound is considered the major challenge. However, choosing a catalyst with a suitable structure and composition can overcome this challenge and increase the production of cinnamyl alcohol. The type of catalyst plays an important role in the present reaction because they can increase the selectivity of cinnamyl alcohol (CALC). Important factors affecting activity and selectivity include the active metal, the properties of the catalyst support, and the particle size of the metal. Pt/SiO_2 was a selective catalyst of the series toward cinnamyl alcohol; achieving high selectivity to hydrogenation of the C=O functionality over the active sites is challenging. While Pt catalysts favor this over hydrogenation of the C=C functionality, subsequent hydrogenation results in the production of hydrocinnamyl alcohol as a byproduct [1–3].

The selectivity of cinnamaldehyde hydrogenation to cinnamyl alcohol (CALC) has been extensively studied [1–23]; however only a few kinetic studies have investigated the reaction kinetics of cinnamaldehyde hydrogenation.

The most common model proposed to describe this reaction mechanism is the Langmuir–Hinshelwood model (LHM) (or Langmuir–Hinshelwood–Hougen–Watson (LHHW) model). For example, Mohire and Yadav [26] studied the hydrogenation of cinnamaldehyde to hydrocinnamaldehyde over a 5% Ni–Cu catalyst and assumed that cinnamaldehyde and H_2 both adsorbed on the vacant surface sites. By calculating the reaction rate constants at different temperatures, the activation energy was observed to be 52.05 kJ/mol. Elsewhere, Hajek and Murzin [27] calculated an activation energy of ~34 kJ/mol for cinnamaldehyde hydrogenation over a Ru-5% Sn/SiO_2 catalyst. Although a plausible description of the concentration dependencies was obtained via fitting to the Langmuir–Hinshelwood model, the model failed to fit the selectivity dependence.

In contrast, Khan et al. [1] and Neri et al. [28] described the effect of various operating parameters on the reaction kinetics of liquid-phase cinnamaldehyde hydrogenation over both a 5% Pt/C and a Ru/Al_2O_3 catalyst. The authors employed the LHM; however they assumed that both the adsorption and hydrogenation of C=O and C=C groups occur at different active sites with the competitive adsorption of reactants and products. Adsorption and hydrogenation of the C=O bond increases the selectivity to cinnamyl alcohol.

Yamada et al. [29] studied the reaction rate for the hydrogenation of cinnamaldehyde over Pd/C and Pt/C catalysts using aqueous potassium hydroxide solution as a promoter. The reaction rate was observed to be of zero-order with respect to the unsaturated aldehydes. Liu et al. [30] achieved high conversions (>99.9%) and high selectivity (>99.9%) when employing an $AlCl_3$–Pd/C dual catalyst at ambient temperature and atmospheric pressure. The estimated Langmuir–Hinshelwood kinetic model indicated that the reaction was zero-order in cinnamaldehyde, whereas it was first-order in hydrogen.

The reaction rate is controlled by the mass transfer of the reactant from the bulk liquid phase to the surface of the catalyst particles if external liquid-solid mass transfer limitations exist [31]. Toebes et al. [32] used a single-site model incorporating both Langmuir–Hinshelwood kinetics and mass transfer to describe the hydrogenation of cinnamaldehyde over a carbon nanofiber-platinum catalyst. They detected that the intrinsic reaction rate grew by a factor of 120 with the removal of the oxygen-containing surface groups.

In summary, the literature reveals that different kinetic models have been used to describe the consecutive hydrogenation of cinnamaldehyde; however, these kinetic models are diverse in mechanism, and hence in the accuracy of their representation of the experimental results. Therefore, the present work aims to mathematically model of the reaction kinetics of cinnamaldehyde hydrogenation over a commercial 5% Pt/SiO_2 catalyst. The main objective of this study is to increase the production of cinnamyl alcohol, which appears as an intermediate product with hydrocinnamaldehyde, by hindering the hydrogenation reactions that lead to its conversion to hydrocinamyl alcohol. In addition, this research will predict the kinetic parameters of the Langmuir–Hinshelwood model by employing two mathematical models: bulk and intraparticle diffusion. The proposed mathematical model deals with two types of active sites, namely, the acidic sites and the metallic sites represented by the platinum loaded on the surface of the SiO_2 catalyst. The model in this study suggests that there is an abundance of hydrogen gas and therefore the competition between hydrogenation/dehydrogenation reactions taking place on active sites and on the other hand the state of non-competition has been taken into account.

2. Experimental Work

Experiments were conducted using a 300 cm^3 stainless steel batch reactor (Parr Instrument Company, USA) equipped with a pressure gauge, stirrer, and heater to control the

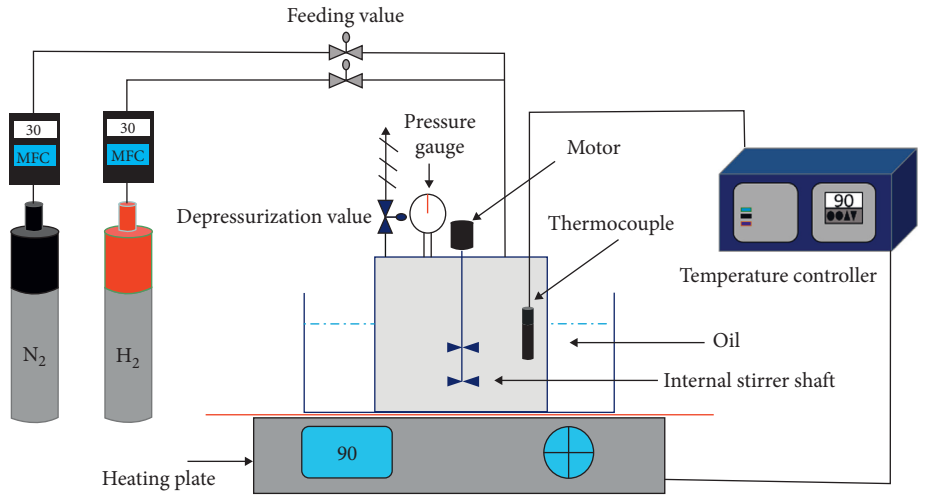

Figure 2: Scheme of the batch reactor.

temperature, which was monitored via a thermocouple, as shown in Figure 2. A commercial 5% Pt/SiO_2 (Escat 2351) catalyst supplied by Strem Chemicals (USA) was employed directly without further modification (gray powder, particle size = 40 μm, surface area = 400 m^2/g). Ethanol (Sigma-Aldrich, USA) was used as the solvent. For a typical experiment, 0.1 g of catalyst, 10 g of cinnamaldehyde (99% GC purity, purchased from Sigma-Aldrich), and 190 mL of solvent were introduced into the reactor. The reactor was then flushed three times with 5 bar nitrogen; the temperature was increased moderately to the required value (90–110°C) using heating oil; and the pressure of hydrogen was raised to the desired value (10–30 bar). A reactor was equipped with a pressure control valve which was used to control the reactor pressure by regulating the hydrogen being fed to the reactor until the desired operating conditions were reached. Mass transfer can play an important role in liquid-phase hydrogenations using porous catalysts. Therefore, it is critically important that mass transfer effects are ruled out before attempting to obtain reliable kinetic data. In order to reduce the chances of mass transfer limitations, the smallest catalyst particle sizes (<150 μm) and highest stirring speed were used (1600 rpm). These two factors increase the rate of mass transfer from the gas to the liquid phase, increase the rate of reactant transfer from the bulk liquid to the catalyst surface, and minimize internal diffusion resistance.

Samples were withdrawn at regular intervals and analyzed by offline gas chromatography with a flame ionization detector (FID) (Agilent 6890N, USA), employing a Rtx-1 capillary column (30-m length, 0.25-mm ID, and 0.25-μm film thickness), with nitrogen as the carrier gas. The relative standard error was estimated by repeating a specific experiment three times and calculated as ±1%.

3. Mathematical Modelling

3.1. Bulk Model. Bulk models assumed that (i) each point on the interior of the catalyst surface is accessible to the same concentration [33] and (ii) mixing provides a uniform distribution of liquid and catalyst particles. The adsorption reaction kinetic models suggest that the adsorption rate of the solute on the surface of the adsorbent has the dominant influence on the adsorption kinetics; therefore, the exterior mass transfer and intraparticle diffusion can be considered negligible [34].

For the reaction pathway shown in Figure 1, the set of differential equations (1) to (4) expresses the concentration change in the bulk liquid for the four components [27]:

$$\frac{dc_{CALD}}{dt} = -\frac{W_c}{V_R}(r_1 + r_2), \quad (1)$$

$$\frac{dc_{CALC}}{dt} = \frac{W_c}{V_R}(r_1 - r_3), \quad (2)$$

$$\frac{dc_{HALD}}{dt} = \frac{W_c}{V_R}(r_2 - r_4), \quad (3)$$

$$\frac{dc_{HALC}}{dt} = \frac{W_c}{V_R}(r_3 - r_4). \quad (4)$$

3.2. Intraparticle Diffusion Model. Two steps summarize the intraparticle diffusion model, including diffusion of the reactant molecules: firstly at the bulk external film, and secondly between the exterior film and the surface of catalyst, where the reaction occurs [35]. If external liquid-solid mass transfer limitation is negligible and the internal diffusion effects are significant, then the concentration gradient across the catalyst pellet must be taken into consideration in determining the net reaction rate. A rigorous mathematical model was developed for a diffusion-reaction process in a spherical catalyst pellet contained in an isothermal batch reactor.

3.2.1. Mass Balance in the Bulk Liquid. The mass balance of the bulk liquid is expressed below [32]:

$$\frac{dc_{b,j}}{dt} = -\frac{A_P}{V_{Liq}} D_j \frac{\partial c_{b,j}}{\partial r}\Big|_{r=r_P}, \tag{5}$$

$$A_P = \frac{3}{r_p} V_P. \tag{6}$$

3.2.2. Mass Balance in the Catalyst Particle. The mass balance inside the catalyst particle is given by [36–38]

$$\varepsilon_P \frac{dc_{pj,i}}{dt} = D_{\text{eff},j}\left(\frac{d^2 c_{pj,i}}{dr^2} + \frac{2}{r}\frac{dc_{pj,i}}{dr}\right) + (1-\varepsilon_P)\nu_j \rho_{\text{cat}} R_{r,j}. \tag{7}$$

Equation (7) has been discretized by a finite difference method based on a three-point centered scheme for the second-order derivative.

$$\varepsilon_P \frac{dc_{Pj,i}}{dt} = D_{\text{eff}}\left(\frac{c_{Pj,i+1} - 2c_{Pj,i} + c_{i-1}}{\Delta r^2} + \frac{2}{r_i}\frac{c_{Pj,i+1} - c_{Pj,i-1}}{2\Delta r}\right) + (1-\varepsilon_P)\nu_j \rho_{\text{cat}} R_{r,j}. \tag{8}$$

with boundary conditions

$$\begin{aligned} &\text{at} r = 0, \quad \frac{dc_{P,j}}{dr} = 0, \\ &\text{at} r = r_P, \quad c_{Pj,i} = c_{Pj,i}(r = r_P). \end{aligned} \tag{9}$$

where j represents the component index and i represents the radial position inside the reactor particles. Equation (8) has been generalized for five components within the reaction mixture.

The reactant concentrations around the catalyst particle is assumed to be equal to the reactant concentrations in the bulk. The Wilke–Chang equation (equation (9)) was used to determine the diffusion coefficient for a dilute solute j [39, 40]:

$$\mathrm{D}^o_{j,m} = 7.4 \times 10^{-8} \sum_{\substack{j=1 \\ j \neq A}}^{N_C} \frac{\left(x_j \varnothing_j M w_j\right)^{0.5} T}{\mu \left(V_A\right)^{0.6}}. \tag{10}$$

For the multicomponent liquid mixture, the diffusivity of compound j was estimated, as per equation (10) [41]:

$$Dj = \varepsilon_P \frac{D^{\circ}_{j,m}}{\tau}. \tag{11}$$

Rigorous mathematical modelling involves solving the differential equations of the reactant concentrations in bulk liquid and inside catalyst particle.

4. Reaction Kinetic Models

Two main reasons make employing a batch reactor better than a continuous reactor for reaction kinetic studies. First, in a batch reactor, the changes in the reactant concentrations can be measured instantaneously, whereas the continuous reactor provides only the final concentrations. Second, in a batch reactor, the reaction temperature is controlled accurately, allowing for a precise description of the reaction rate constant with respect to temperature. Selecting an accurate kinetic model is essential for the optimal representation of the experimental results and thus for a better design that optimizes the process. In addition, accurate kinetic models can maximize the selectivity of the desired products. Although many researchers have investigated cinnamaldehyde hydrogenation over different types of catalysts using the Langmuir–Hinshelwood model to fit the experimental data, no comparative study has distinguished between these kinetic models. Zamostny and Belohlav [42] used a simplified Langmuir–Hinshelwood kinetic model to fit experimental data of cinnamaldehyde hydrogenation. Hydrogen pressure was not taken into consideration in the kinetic modelling and the adsorption coefficient was assumed to be independent of temperature. Hajek and Murzin [27] employed a Langmuir–Hinshelwood reaction mechanism with the assumption of different adsorption sites for organic compounds and hydrogen. Virtanen et al. [43] used the Langmuir–Hinshelwood–Hougen–Watson concept to represent cinnamaldehyde hydrogenation, assuming competitive adsorption of all compounds with dissociative hydrogen adsorption. Single-site Langmuir–Hinshelwood kinetic model including mass transfer effects was developed by Toebes et al. [32]. It was assumed that no competition takes place with hydrogen adsorption, which is assumed to occur dissociatively. A two-site Langmuir-Hinshelwood kinetic model was developed by Khan et al. [1]. This model considered the effect of various operating parameters (catalyst loading, partial pressure of hydrogen, and initial substrate concentration) on the rates of hydrogenation. A summary of previously investigated kinetic models is presented in Table 1 in order to facilitate comparison.

The Arrhenius equation was employed to elucidate the relationship between the reaction rate constant (k) and the reaction temperature.

$$k_i = A_{o,i} \exp\left(-\frac{E_i}{RT}\right). \tag{12}$$

It was assumed that the adsorption equilibrium constants do not depend on temperature.

As seen in Figure 1, the reaction kinetic model of the present study (RKP) was investigated by employing Langmuir–Hinshelwood kinetics. The goal was to reach the optimal reaction mechanism that results in the largest production of cinnamyl alcohol. However, throughout the experiments, small amounts of hydrocinnamicaldehyde (HCNAL) were detected in the bulk solvent. Reaction modelling requires that the reaction pathway of cinnamaldehyde to hydrocinnamaldehyde, as well as hydrocinamyl alcohol, be included in the model.

The model assumed that the adsorption of reactants and products is reversible and competitive while hydrogen is

Table 1: Reaction kinetic models for the liquid-phase hydrogenation of cinnamaldehyde.

Kinetic model	Authors	Abbre-viation
$r_1 = k_1 C_{CALD}/(C_{CALD} + (K_{CALC}/K_{CALD})C_{CALC}) + ((K_{HALD}/K_{CALD})C_{HALD}) + ((K_{HALC}/K_{CALD})C_{HALC}))$ $r_2 = k_2 C_{CALD}/(C_{CALD} + (K_{CALC}/K_{CALD})C_{CALC}) + ((K_{HALD}/K_{CALD})C_{HALD}) + ((K_{HALC}/K_{CALD})C_{HALC}))$ $r_3 = (k_3 (K_{CALC}/K_{CALD})C_{CALC})/((C_{CALD} + (K_{CALC}/K_{CALD})C_{CALC}) + ((K_{HALD}/K_{CALD})C_{HALD}) + ((K_{HALC}/K_{HALC})C_{HALC}))$ $r_4 = (k_4 (K_{HALD}/K_{CALD})C_{HALD})/((C_{CALD} + (K_{CALC}/K_{CALD})C_{CALC}) + ((K_{HALD}/K_{CALD})C_{HALD}) + ((K_{HALC}/K_{CALD})C_{HALC}))$	Zamostny and Belohlav [42]	RK1
$r_1 = (k_1 K_{CALD} K_{H_2} C_{CALD} p_{H_2})/(1 + K_{CALD} C_{CALD} + K_{CALC} C_{CALC} + K_{HALD} C_{HALD} + K_{HALC} C_{HALC})(1 + K_{H_2} p_{H_2}))$ $r_2 = (k_2 K_{CALD} K_{H_2} C_{CALD} p_{H_2})/(1 + K_{CALD} C_{CALD} + K_{CALC} C_{CALC} + K_{HALD} C_{HALD} + K_{HALC} C_{HALC})(1 + K_{H_2} p_{H_2}))$ $r_3 = (k_3 K_{CALC} K_{H_2} C_{CALC} p_{H_2})/(1 + K_{CALD} C_{CALD} + K_{CALC} C_{CALC} + K_{HALD} C_{HALD} + K_{HALC} C_{HALC})(1 + K_{H_2} p_{H_2}))$ $r_4 = (k_4 K_{HALD} K_{H_2} C_{HALD} p_{H_2})/(1 + K_{CALD} C_{CALD} + K_{CALC} C_{CALC} + K_{HALD} C_{HALD} + K_{HALC} C_{HALC})(1 + K_{H_2} p_{H_2}))$	Hajek and Murzin [27]	RK2
$r_1 = (k_1 K_{CALD} K_H C_{CALD} p_{H_2} f_{DA})/((1 + K_{CALD} C_{CALD} + K_{CALC} C_{CALC} + K_{HALD} C_{HALD} + K_{HALC} C_{HALC} + \sqrt{K_H p_{H_2}})^3)$ $r_2 = (k_2 K_{CALD} K_H C_{CALD} p_{H_2} f_{DA})/((1 + K_{CALD} C_{CALD} + K_{CALC} C_{CALC} + K_{HALD} C_{HALD} + K_{HALC} C_{HALC} + \sqrt{K_H p_{H_2}})^3)$ $r_3 = (k_3 K_{CALC} K_H C_{CALC} p_{H_2} f_{DA})/((1 + K_{CALD} C_{CALD} + K_{CALC} C_{CALC} + K_{HALD} C_{HALD} + K_{HALC} C_{HALC} + \sqrt{K_H p_{H_2}})^3)$ $r_4 = k_4 K_{HALD} K_H C_{HALD} p_{H_2} f_{DA}/((1 + K_{CALD} C_{CALD} + K_{CALC} C_{CALC} + K_{HALD} C_{HALD} + K_{HALC} C_{HALC} + \sqrt{K_H p_{H_2}})^3)$ $f_{DA} = f_{DA} + (1 - f_{DA})\exp(-k_{DA} t_{cumu})$	Virtanen et al. [43]	RK3
$r_1 = ((k_1 K_{CALD} C_{CALD}/1 + K_{CALD} C_{CALD} + K_{CALC} C_{CALC} + K_{HALD} C_{HALD} + K_{HALC} C_{HALC}) \times (K_H C_{H_2}/(1 + \sqrt{K_H C_{H_2}})))$ $r_2 = (k_2 K_{CALD} C_{CALD}/1 + K_{CALD} C_{CALD} + K_{CALC} C_{CALC} + K_{HALD} C_{HALD} + K_{HALC} C_{HALC}) \times (\sqrt{K_H C_{H_2}}/1 + \sqrt{K_H C_{H_2}}))$ $r_3 = (k_3 K_{CALC} C_{CALC}/1 + K_{CALD} C_{CALD} + K_{CALC} C_{CALC} + K_{HALD} C_{HALD} + K_{HALC} C_{HALC}) \times (\sqrt{K_H C_{H_2}}/1 + \sqrt{K_H C_{H_2}}))$ $r_4 = (k_4 K_{HALD} C_{HALD}/1 + K_{CALD} C_{CALD} + K_{CALC} C_{CALC} + K_{HALD} C_{HALD} + K_{HALC} C_{HALC}) \times (\sqrt{K_H C_{H_2}}/1 + \sqrt{K_H C_{H_2}}))$	Toebes et al. [32], Handjani et al. [25]	RK4
$r_1 = ((k_{01} K_{CALD} C_{CALD} (k_H p_{H_2}) w)/(1 + (k_1/k_{01}) C_{CALD}))$ $r_2 = ((k_{02} K_{CALD} C_{CALD} (k_H p_{H_2}) w)/(1 + (k_2/k_{02}) C_{CALD}))$ $r_3 = (((k_{03} K_{CALC} C_{CALC}) (k_H p_{H_2}) w)/(1 + (k_3/k_{03}) C_{CALC}))$ $r_4 = ((k_{04} K_{HALD} C_{HALD} (k_H p_{H_2}) w)/(1 + (k_4/k_{04}) C_{HALD}))$	Khan et al. [1]	RK5

activated on different sites and does not compete with the organic compounds (hydrogen shows non-competitive and dissociative adsorption). So adsorption and desorption are considered to be in quasi-equilibrium. The rate-determining step is considered to be the reaction between atomic hydrogen and the adsorbed organic compound. Therefore, a one site model was investigated. In this model, C=C and C=O are hydrogenated on the same type of site, as shown below:

$$r_1 = \frac{K_1 K_A C_A}{1 + K_A C_A + K_B C_B + K_C C_C + K_D C_D} \times \frac{\sqrt{K_H . C_{H_2}}}{1 + \sqrt{K_H . C_{H_2}}}, \tag{13}$$

$$r_2 = \frac{K_2 K_A C_A}{1 + K_A C_A + K_B C_B + K_C C_C + K_D C_D} \times \frac{\sqrt{K_H . C_{H_2}}}{1 + \sqrt{K_H . C_{H_2}}}. \tag{14}$$

$$r_3 = \frac{K_3 K_B C_B}{1 + K_A C_A + K_B C_B + K_C C_C + K_D C_D} \times \frac{\sqrt{K_H . C_{H_2}}}{1 + \sqrt{K_H . C_{H_2}}}, \tag{15}$$

$$r_4 = \frac{K_4 K_C C_C}{1 + K_A C_A + K_B C_B + K_C C_C + K_D C_D} \times \frac{\sqrt{K_H . C_{H_2}}}{1 + \sqrt{K_H . C_{H_2}}}. \tag{16}$$

A: cinnamaldehyde, *B*: cinnamyl alcohol, *C*: hydrocinnamaldehyde, *D*: hydrocinnamal alcohol.

Because the present study was conducted at high pressure, the hydrogen term is neglected because the order associated with hydrogen is zero, so the value of the numerator is equal to the value of the denominator. Therefore, the limit of hydrogen will be one, as shown in the following:

$$r_1 = \frac{K_1 K_A C_A}{1 + K_A C_A + K_B C_B + K_C C_C + K_D C_D}, \tag{17}$$

$$r_2 = \frac{K_2 K_A C_A}{1 + K_A C_A + K_B C_B + K_C C_C + K_D C_D}, \tag{18}$$

$$r_3 = \frac{K_3 K_B C_B}{1 + K_A C_A + K_B C_B + K_C C_C + K_D C_D}, \tag{19}$$

$$r_4 = \frac{K_4 K_C C_C}{1 + K_A C_A + K_B C_B + K_C C_C + K_D C_D}. \tag{20}$$

5. Computational Method

The kinetic parameters were estimated from experimental data by means of a nonlinear dynamic optimization algorithm, in which results of the mathematical model were compared against the experimental information. Six experiments at different operating conditions were simulated for each reaction mechanism, and the mean absolute error (MAE) was estimated by comparing the simulation concentrations with the predicted experimental concentrations. The MAE was calculated according to equation (20) [44, 45].

$$\mathrm{MAE} = \frac{1}{N \times M} \sum_{j=1}^{M} \sum_{i=1}^{N} \left| c_{i,j}^{\mathrm{exp}} - c_{i,j}^{\mathrm{pred}} \right|. \quad (21)$$

The ordinary differential equations governing the reactor and kinetic models were solved using the fourth-order Runge–Kutta method, while a Genetic Algorithm (GA) optimization stochastic technique was used to predict the kinetic parameters by minimizing the objective function (minimum MAE). The simulation results that were obtained from the constructed kinetic models were compared with relevant experimental results, until the model was capable of reaching reasonable results.

Genetic Algorithms are powerful and widely applicable stochastic search and optimization methods based on the concepts of natural selection and natural evaluation [46]. Genetic Algorithms apply the principles of survival of the fittest, selection, reproduction, crossover, and mutation of individuals to obtain a new and better individual (i.e., new solutions). Crossover is implemented by selecting a random point on the chromosome where the parents' parts exchange happens. The crossover then brings up a new offspring based on the exchange point chosen with particular parts of the parents. Normally, mutation takes place after crossover is done. This operator applies the changes randomly to one or more "genes" to produce a new offspring, so it creates new adaptive solutions which avoid local optima. Within the selection stage, individual genomes are chosen from a population for later breeding [47].

A nonlinear constraint was imposed on the variable's candidate for optimization to limit the GA search span to gain acceptable kinetic parameters. Table 2 shows the parameters used in the Genetic Algorithm optimization. All computations within this study were performed using MATLAB software version 2015a.

Table 2: Genetic algorithm parameters.

Population size	10
Maximum generation	1000
Crossover probability	0.8
Mutation probability	0.4
Neighborhood size	0.05

6. Results and Discussion

6.1. Comparison between Kinetic Models. Nonlinear optimization was used to predict the kinetic parameters of five models and compared with the methodology used in the present study. This method covered the change in the initial cinnamaldehyde concentration, temperature, and pressure on the rate of reaction for all experiments simultaneously. In fact, nonlinear optimization is more accurate than another traditional method which estimates the kinetics parameters via the linearized Arrhenius equation (ln k verses $1/T$). Figure 3 illustrates the priority curves obtained for the model of the present study and five Langmuir–Hinshelwood kinetic models, where the points clustered around the diagonal line indicate the validity of these five kinetic models. Figures 3(a) and 3(g) show a divergence between the experimental and predicted results, especially for CALD; however, the other figures demonstrate an acceptable convergence. The values of the predicted errors for the present modified model and the five tested reaction kinetics are summarized in Table 3. In general, the accuracy of the obtained results increases with an increasing number of factors in the empirical equation, in which the kinetic models RKP, RK2, RK3, and RK4 have more factors (e.g., adsorption factors) than RK1 and RK5; therefore, the estimated error (MAE) for these three models (≈2.3, 2.3, 2.5 and 2.3 mol/m^3, respectively) is lower than for the other two models (≈3.1 and 3.6 mol/m^3, respectively). The MAE obtained by the RKP, RK2, and RK4 kinetic models were approximately equal and were smaller than that obtained by the other three kinetic models. Indeed, RK2 and RK4 have approximately the same main factors, except for the term that represents hydrogen pressure, which is equal to 1 for RK2 but is 0.5 for RK4. The estimated error for RK4 was slightly lower than for RK2 and identical to RKP, and this supports the assumption that there is a single-site for the adsorption of hydrogen molecules in the RK4 kinetic model and RKP compared with the dual-site adsorption for hydrogen molecules in the RK2 kinetic model.

When comparing the RKP model in the present study, which is directed towards the production of cinnamyl alcohol, it is noticed that there is a difference from the reaction mechanism of the RK3 model, which is directed towards the production of hydrocinnamaldehyde. Therefore, the results of the RKP model suggest that the non-competitive hypothesis for components is better than the competitive hypothesis, while the RK3 model showed that the competitive hypothesis is better. On the other hand, RK2 and RK4 models only used the non-competitive hypothesis and neglected the competitive hypothesis. The present study, which used both hypotheses, demonstrated a consistency with the trend of RK2 and RK4 models by favoring the non-competitive hypothesis over the competitive hypothesis. Furthermore, the MAE results of the RKP model in the competitive and non-competitive hypotheses are 2.8233 and 2.3022 mol/m^3, respectively; these reinforce the fact that the non-competitive hypothesis is preferable. In other words, the error has been reduced by about 18%.

The present model suggests that the use of Pt as a metal support through the hydrogenation of the reaction of cinnamaldehyde contributes to an increase in the production of cinnamyl alcohol and makes it the main product. The addition of Pt reduces the free active sites of the catalyst by poisoning some or most of them according to the loading

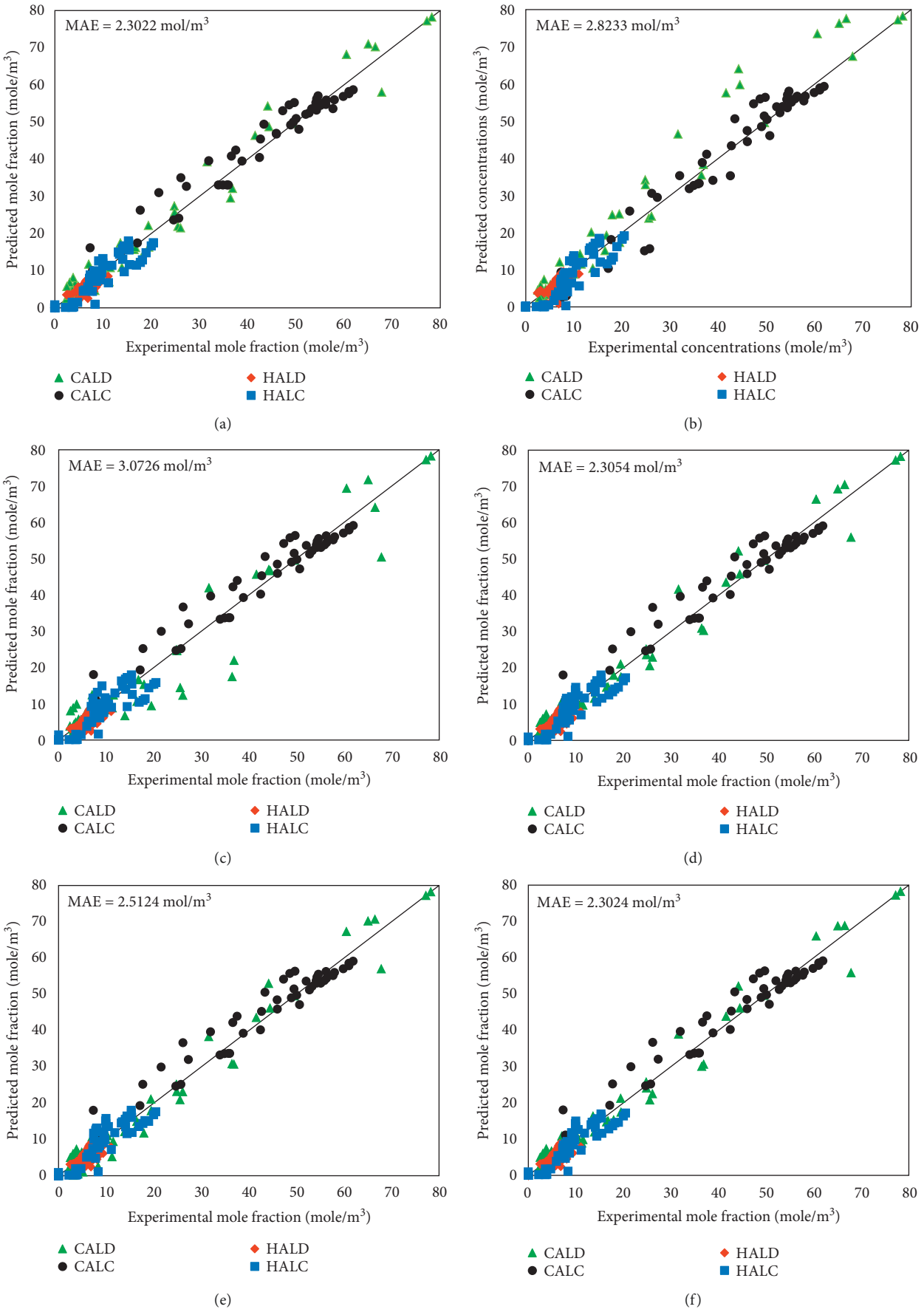

Figure 3: Continued.

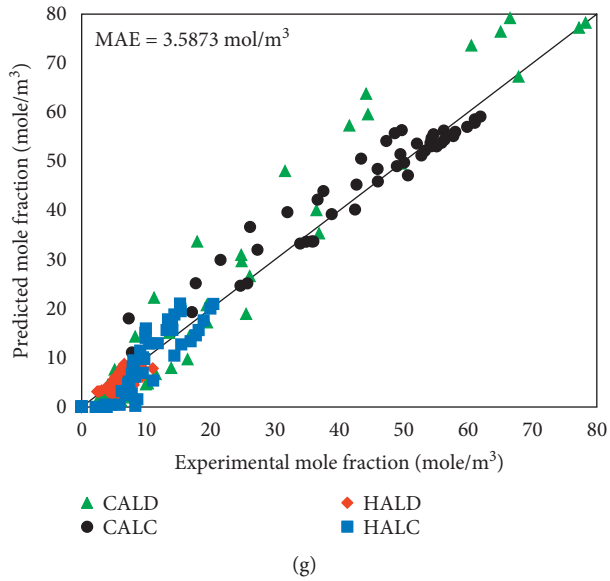

(g)

Figure 3: Parity diagram indicating the calculated molar fractions obtained by the bulk model versus the experimental molar fractions for all experiments and components. Modelling results have been obtained using the reaction mechanism (a) (RKP-non-competitive), (b) (RKP-competitive), (c) (RK1), (d) (RK2), (e) (RK3), (f) (RK4), and (g) (RK5).

Table 3: Summary of the estimated errors.

Kinetic model	MAE (mol/m^3)
RKP-non-competitive	2.3022
RKP-competitive	2.8233
RK1	3.0726
RK2	2.3054
RK3	2.5124
RK4	2.3024
RK5	3.5873

ratio and due to the formation of hydrocinnamyl alcohols occurring at the free catalytic sites. Therefore, the selectivity of cinnamyl alcohol will increase and the hydrogenation of cinnamyl alcohol will decrease. Assuming different adsorption sites for organic compounds and hydrogen, the role of hydrogen adsorption in hydrogenation processes is interesting. On the one hand, it is known that hydrogen absorbs on noble metals; on the other hand, hydrogen molecules are much smaller than organic molecules, especially in the present case. This means that the interstitial sites between the adsorbed organic molecules remain available for hydrogen adsorption. Thus, the adsorption behavior turns into a non-competitive one. Therefore, the RK4 model was found to be better than the other four models in representing the consecutive hydrogenation of cinnamaldehyde to other products.

6.2. Comparison between Bulk and Intraparticle Diffusion Models. Cinnamaldehyde hydrogenation was carried out at temperature range 90–110°C, with a pressure range between 10 and 30 bar, using ethanol as a nonpolar solvent. Cinnamyl alcohol, hydrocinnamaldehyde, and hydrocinnamyl alcohol are the principal products that result from this reaction. Figure 4 compares the experimental results and the bulk model results using the optimum kinetic model (RKP), while Figure 5 presents a comparison between the experimental results and intraparticle diffusion model results using the same model. Both figures show a good agreement between the concentrations obtained in the experimental study and those predicted by the theoretical model.

Figures 4 and 5 provide an indication of the behavior that occurs in the hydrogenation of cinnamaldehyde, which appears to follow the behavior of a sequential parallel reaction system. Furthermore, the concentration of cinnamyl alcohol rose rapidly at the start of the reaction and then became almost constant after 200 min, similar to previous results [8]. The concentration of hydrocinnamaldehyde however slightly decreased after 50 min of reaction time. Hajek and Murzin [27] observed the same behavior, where the selectivity of hydrocinnamaldehyde decreased slightly over time.

Figure 6 presents a comparison between the estimated molar fractions obtained by the bulk and intraparticle diffusion models versus the experimental molar fractions for all experiments and components. There was good conformity between the experimental and theoretical results, as illustrated in the value of the absolute error that was determined according to the consistency between the practical and predicted mole fractions. In spite of employing the same kinetic model (RK present) for both bulk and intraparticle diffusion models, the bulk model showed a slightly low level of error (2.3 mol/m^3) compared with the intraparticle model (2.33 mol/m^3). This can be attributed to the error corresponding to the intraparticle mass transfer coefficient calculations.

The kinetic parameters of the reaction (RKP) for both the bulk and intraparticle diffusion models were determined by benchmarking against the experimental results. Table 4

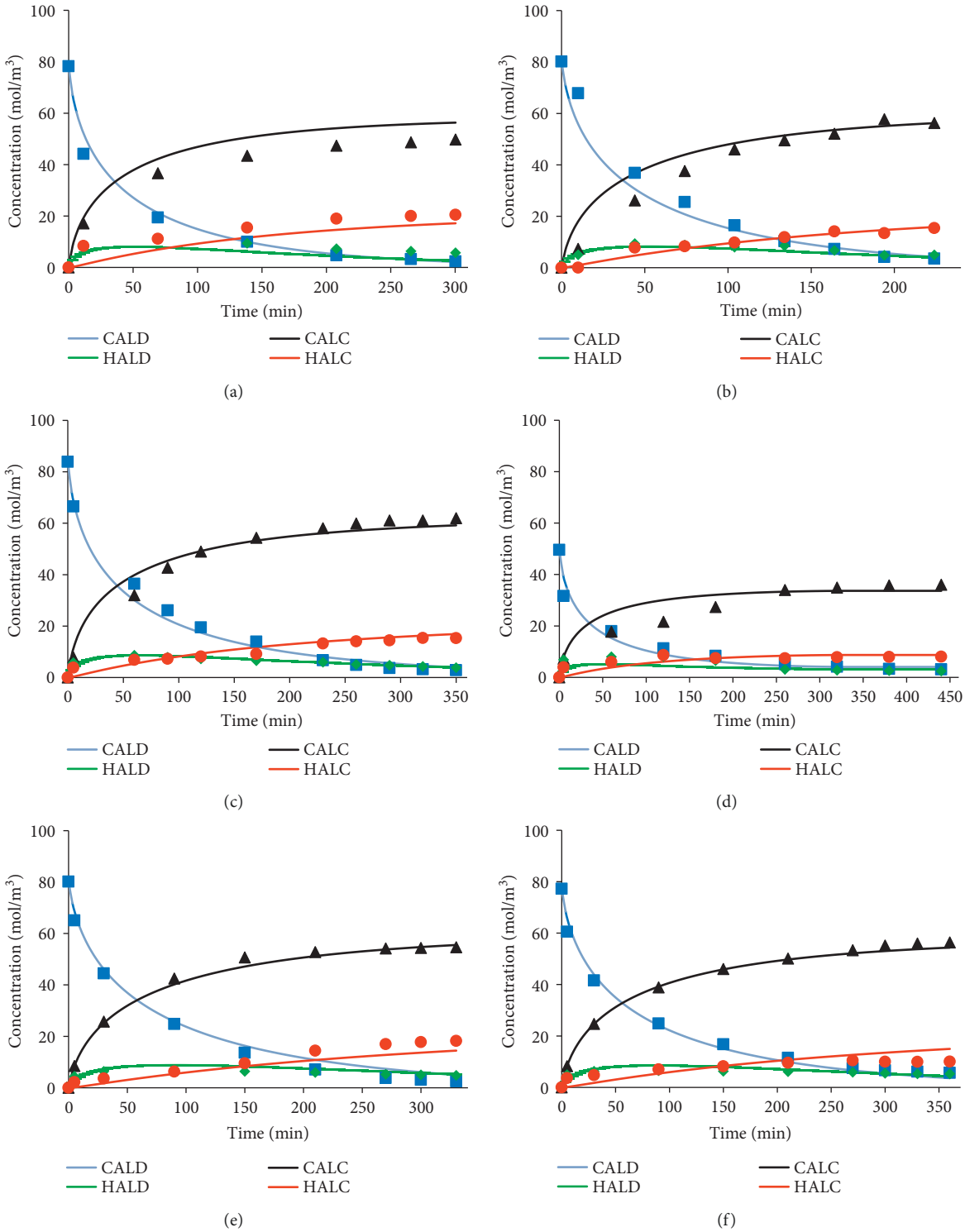

Figure 4: Comparison between the experimental and bulk model results. Experimental conditions are (a) ($T = 110^{\circ}$C, P = 30 bar, initial CALD concentration = 78.25 mol/m^3), (b) ($T = 110^{\circ}$C, P = 30 bar, initial CALD concentration = 80.19 mol/m^3), (c) ($T = 110^{\circ}$C, P = 20 bar, initial CALD concentration = 83.88 mol/m^3), (d) ($T = 110^{\circ}$C, P = 30 bar, initial CALD concentration = 49.57 mol/m^3), (e) ($T = 90^{\circ}$C, P = 30 bar, initial CALD concentration = 80.15 mol/m^3), and (f) ($T = 90^{\circ}$C, P = 30 bar, initial CALD concentration = 77.23 mol/m^3).

displays the estimated values of the pre-exponential factor and apparent activation energy (Ea). Despite there being a considerable difference between the kinetic parameters calculated using the two different mathematical models, the observed MAE for both models was very similar. This can be attributed to using fine catalyst particles (40 μm), which significantly reduces the influence of mass transfer effects; therefore the variation in concentration through the catalyst

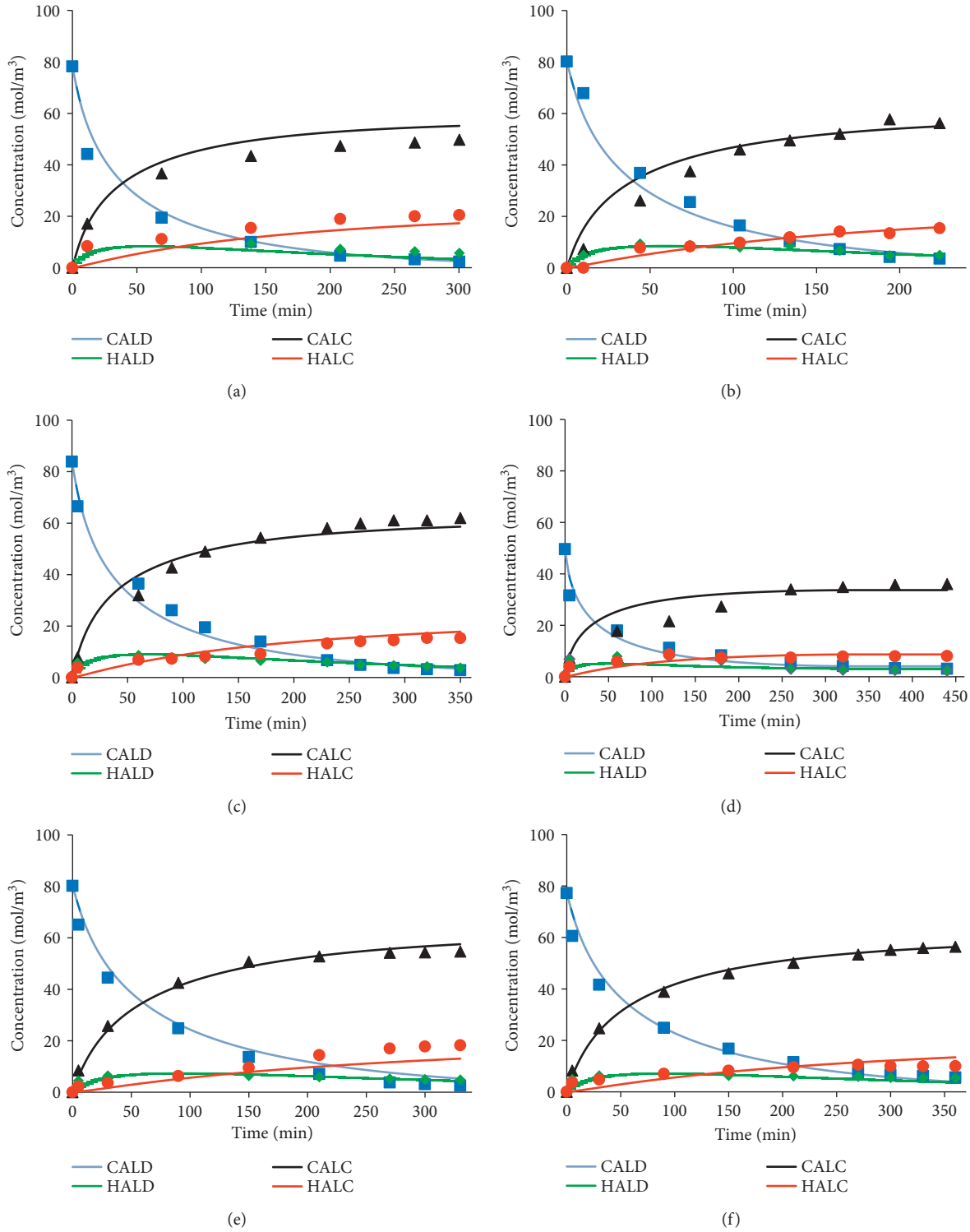

Figure 5: Comparison between the experimental and intraparticle diffusion model results. Experimental conditions are (a) ($T = 110^{\circ}C$, $P = 30$ bar, initial CALD concentration = 78.25 mol/m^3), (b) ($T = 110^{\circ}C$, $P = 30$ bar, initial CALD concentration = 80.19 mol/m^3), (c) ($T = 110^{\circ}C$, $P = 20$ bar, initial CALD concentration = 83.88 mol/m^3), (d) ($T = 110^{\circ}C$, $P = 10$ bar, initial CALD concentration = 49.57 mol/m^3), (e) ($T = 90^{\circ}C$, $P = 30$ bar, initial CALD concentration = 80.15 mol/m^3), and (f) ($T = 90^{\circ}C$, $P = 30$ bar, initial CALD concentration = 77.23 mol/m^3).

particles is small. This conclusion is supported by the work of Zhu and Zaera [5], who found that the elementary hydrogenation selectivity was independent of the particle size, especially when the size was less than 250 μm. The values of the activation energy for cinnamaldehyde hydrogenation to cinnamyl alcohol were 24.33 and 31.35 kJ/mol for the bulk

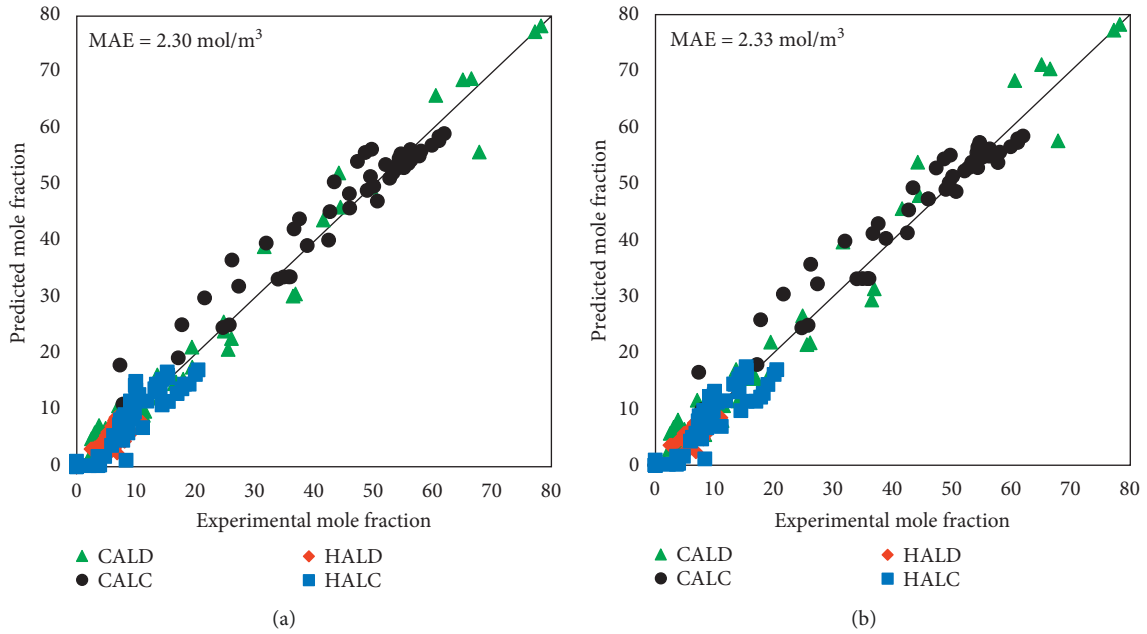

Figure 6: Parity diagram indicating the calculated molar fractions obtained by the (a) bulk and (b) intraparticle diffusion models versus the experimental molar fractions for all experiments and components.

and intraparticle diffusion models, respectively. These results approached the value of the activation energy (31.4 kJ/mol) obtained by Hajek and Murzin [27] for cinnamaldehyde hydrogenation employing a Ru-5% Sn/Sol-Gel catalyst, and by Mohire and Yadav [26], who obtained an activation energy of approximately 52 kJ/mol for the hydrogenation of cinnamaldehyde over a 5% Ni–Cu catalyst. From inspection of Table 4 and Figures 4 and 5, it is seen that the product in the greatest concentration was cinnamyl alcohol. Furthermore, there was a good agreement between the estimated and experimental concentrations. The activation energy of cinnamyl alcohol hydrogenation (≈152 kJ/mol) was significantly higher than that of cinnamaldehyde reduction (≈24 kJ/mol). This therefore limits the further hydrogenation of cinnamyl alcohol to form hydrocinnamyl alcohol. This result is similar to that obtained by Khan et al. [1].

As shown in Figure 1, there are two reaction routes to obtain hydrocinnamyl alcohol. Either the cinnamaldehyde hydrogenates to cinnamyl alcohol, and then to hydrocinnamyl alcohol; or, the cinnamaldehyde hydrogenates to hydrocinnamaldehyde, and then to hydrocinnamyl alcohol. If internal mass transfer limitations exist, the observed reaction rate is influenced by the diffusion of the reactants (cinnamaldehyde) from the surface to the active sites and reverse diffusion of intermediate and final products (cinnamyl alcohol, hydrocinnamaldehyde, and hydrocinnamyl alcohol) from active sites to the catalyst surface. Therefore, the activation energies for cinnamaldehyde reduction and cinnamaldehyde hydrogenation in the intraparticle diffusion model were higher than the corresponding reactions in the bulk model. In contrast, the activation energies for the cinnamyl alcohol hydrogenation and hydrocinnamaldehyde reduction in the intraparticle diffusion model were lower than the corresponding reactions in the bulk model. This occurred because in the intraparticle model, the two reactions (cinnamaldehyde reduction and cinnamaldehyde hydrogenation) occur after cinnamaldehyde diffuses into the catalyst particles. After this, the intermediate products react, and then the reaction products are liberated from the catalyst as a result of diffusion.

Table 4: Predicted kinetic parameters.

	Parameter	Bulk model	Intraparticle diffusion model
Adsorption constants	K_{CALD}	0.0298	0.067827
	K_{CALC}	0.9514	2.39272
	K_{HALD}	0.1663	0.270205
	K_{HALC}	0.9764	0.929179
	K_{H2}	0.0052	0.233519
Pre-exponential factor	A_{1o}	64.1472	45001.91
	A_{2o}	98.3952	968396
	A_{3o}	534.75	20378.56
	A_{4o}	199.63	12009.24
Activation energy (kJ/mol)	E_1	24.33	31.35
	E_2	28.27	43.96
	E_3	152.59	146.08
	E_4	37.74	34.81

7. Conclusion

The reaction kinetics of the liquid-phase hydrogenation of cinnamaldehyde over a Pt/SiO_2 catalyst were investigated. The modified model and the five kinetic models for cinnamaldehyde hydrogenation were evaluated and compared. The Langmuir–Hinshelwood kinetic model, which assumes a single-site adsorption for hydrogen molecules, was found to best represent the consecutive hydrogenation of cinnamaldehyde. In addition, the prediction of the bulk diffusion

model was compared with the intraparticle diffusion model. The predictions of the intraparticle model (MAE = 2.33 mol/m^3) were very close to those of the bulk model (MAE = 2.30 mol/m^3) due to using a catalyst with a very small particle size (<40 microns). Although the MAE results are convergent, the bulk model is more favorable as it is simpler than the intraparticle model.

Consequently, the present model and the other five kinetic models for cinnamaldehyde hydrogenation were evaluated and compared. The Langmuir–Hinshelwood kinetic model, which assumes a single-site adsorption for hydrogen molecules, was found to best represent the consecutive hydrogenation of cinnamaldehyde. The bulk model is more favorable as it is simpler than the intraparticle model. The study concluded that the non-competitive mechanism between unsaturated hydrogenation reactions to produce intermediate compounds, including cinnamyl alcohol, and saturated hydrogenation reactions to increase the production of either the intermediate compound (i.e., hydrocinnamaldehyde) or the hydrogenation of the intermediate compounds and its complete conversion to hydrocinnamyl alcohol is the most reasonable compared to the case of competitive, which has been proposed in other studies, as there is no competition taking place between hydrogen and dissociative hydrogen adsorption.

The activation energies of cinnamaldehyde hydrogenation to cinnamal alcohol were ~31 kJ/mol and ~24 kJ/mol for the interparticle and the bulk models, respectively. Employing a commercial 5% Pt/SiO_2 catalyst showed a result consistent with previous reports that employed different types of catalysts, although with a lower activation energy of ~24 kJ/mol.

Nomenclature

A_p: External area between the bulk fluid and the particle (m^2/s)
A_o: Pre-exponential factor (mol/gm.cat.min)
c_j: Concentration of component j (mol/m^3)
$c_{b,j}$: Bulk concentration of component j (mol/m^3)
$c_{p,j}$: Concentration of species j inside the particle pores (mol/m^3)
D_j: Effective diffusivity of species j inside the catalyst pores (m^2/s):
$D_{A,\text{Mix}}$: Diffusivity of component A in the mixture (m^2/s)
E_i: Activation energy (J/mol)
f_{DA}: Deactivation parameter
f_{DA}^{∞}: Deactivation parameter at infinite time
k_i: Reaction rate constant (mol/gm cat. min)
k_{deact}: Catalyst deactivation coefficient
K_i: Adsorption constant
N: Components number
M: Experiment number
M_{wj}: Molecular weight of component j (g/mol)
p: Pressure (N/m^2)
p_i: Partial pressure of i component
Rg: Universal gas constant (8.314 j/mol K)
Rr_j: Net rate of the production of species j
r: Particle radial position (m)
r_j: Reaction rate of the production of species (j) (mol/gm.cat min)
r_p: Particle radius (m)
V_p: Total volume of the particles (m^3)
t: Time (min)
t_{cumu}: Cumulative time for catalyst exposure
T: Temperature (K)
V_{Liq}: Total volume of the reactant mixture (m^3)
γ_j: Reaction stoichiometry (–)
W_c: Catalyst weight (gm)
w: Catalyst loading (kg/m^3)
x_j: Liquid-phase mole fraction of component j (–).

Greek letters

ϕ_i: Association factor for the component i (–)
ρ: Gas density (kg/m^3)
μ: Gas viscosity (g/(m s))
Δ: Difference (–)
ε: Void factor (–)
ε_p: Pellet porosity (–)
ρ_{Cat}: Catalyst density (kg/m^3)
τ: Tortuosity factor (–)
μ: Mixture viscosity (kg/m.s).

Subscripts/Superscripts

b: Bulk
CALC: Cinnamyl alcohol
CALD: Cinnamaldehyde
cat: Catalyst
eff: Effective
H_2: Hydrogen
HALC: Hydrocinnamyl alcohol
HALD: Hydrocinnamaldehyde
i: Radial position inside the catalyst particle
j: Number of components
l: Number of experiments
o: Inlet/initial
p: Catalyst particle.

Data Availability

All relevant data are included within the article.

Additional Points

This manuscript provides a logical example of how the basics of chemical engineering can be combined with computational optimization techniques to develop a useful kinetic model, which can be readily used for practical applications on an industrial scale. Five kinetic models for cinnamaldehyde hydrogenation were evaluated and compared. Intraparticle modelling was developed for the liquid-phase hydrogenation of cinnamaldehyde over a commercial Pt/SiO_2.

Conflicts of Interest

The authors declare that they have no conflicts of interest.

References

[1] M. Khan, S. Joshi, and V. Ranade, "Kinetics of cinnamaldehyde hydrogenation in four phase system," *Chemical Engineering Journal*, vol. 377, Article ID 120512, 2019.

[2] Y. Bai, N. Cherkasov, S. Huband, D. Walker, R. Walton, and E. Rebrov, "Highly selective continuous flow hydrogenation of cinnamaldehyde to cinnamyl alcohol in a Pt/SiO_2 coated tube reactor," *Catalysts*, vol. 8, no. 2, p. 58, 2018.

[3] S. Mukherjee and M. A. Vannice, "Solvent effects in liquid-phase reactions: I. activity and selectivity during citral hydrogenation on Pt/SiO2 and evaluation of mass transfer effects," *Journal of Catalysis*, vol. 243, no. 1, pp. 108–130, 2006.

[4] S. Chang, S. Meng, X. Fu, S. Zhang, X. Zheng, and S. Chen, "Hydrogenation of cinnamaldehyde to hydrocinnamyl alcohol on Pt/graphite catalyst," *ChemistrySelect*, vol. 4, no. 7, 2019.

[5] Y. Zhu and F. Zaera, "Selectivity in the catalytic hydrogenation of cinnamaldehyde promoted by Pt/SiO2 as a function of metal nanoparticle size," *Catalysis Science and Technology*, vol. 4, no. 4, pp. 955–962, 2014.

[6] F. F. Abdi, N. Firet, and R. Van De Krol, "Efficient BiVO4Thin film photoanodes modified with cobalt phosphate catalyst and W-doping," *ChemCatChem*, vol. 5, no. 2, pp. 490–496, 2013.

[7] E. Borovinskaya, "Redundancy-free models for mathematical descriptions of three-phase catalytic hydrogenation of cinnamaldehyde," *Catalysts*, vol. 11, no. 2, p. 207, 2021.

[8] Z. M. Shakor, A. A. AbdulRazak, and A. A. Shuhaib, "Optimization of process variables for hydrogenation of cinnamaldehyde to cinnamyl alcohol over a Pt/SiO_2 catalyst using response surface methodology," *Chemical Engineering Communications*, vol. 209, pp. 1–17, 2021.

[9] S. Han, Y. Liu, J. Liv, and R. Li, F. Yuan and Y. Zhu, Improvement effect of Ni to Pd-Ni/SBA-15 catalyst for selective hydrogenation of cinnamaldehyde to hydrocinnamaldehyde," *Catalysts*, vol. 8, no. 5, p. 200, 2018.

[10] Y. Dai, X. Gao, X. Chu et al., "On the role of water in selective hydrogenation of cinnamaldehyde to cinnamyl alcohol on PtFe catalysts," *Journal of Catalysis*, vol. 364, pp. 192–203, 2018.

[11] W. Wang, Y. Xie, S. Zhang, X. Liu, M. Haruta, and J. Huang, "Selective hydrogenation of cinnamaldehyde catalyzed by $ZnO\text{-}Fe_2O_3$ mixed oxide supported gold nanocatalysts," *Catalysts*, vol. 8, no. 2, p. 60, 2018.

[12] R. Dinamarca, R. Espinoza-González, C. Campos, and G. Pecchi, "Magnetic Fe2O3-SiO2-MeO2-Pt (me = Ti, Sn, Ce) as catalysts for the selective hydrogenation of cinnamaldehyde. Effect of the nature of the metal oxide," *Materials*, vol. 12, no. 3, p. 413, 2019.

[13] Z. Cao, J. Bu, Z. Zhong et al., "Selective hydrogenation of cinnamaldehyde to cinnamyl alcohol over BN-supported Pt catalysts at room temperature," *Applied Catalysis A: General*, vol. 578, pp. 105–115, 2019.

[14] G. Wang, H. Xin, Q. Wang, P. Wu, and X. Li, "Efficient liquid-phase hydrogenation of cinnamaldehyde to cinnamyl alcohol with a robust PtFe/HPZSM-5 catalyst," *Journal of Catalysis*, vol. 382, pp. 1–12, 2020.

[15] D. Wang and Y. Zhu, "An effective $Pt\text{-}Cu/SiO_2$ Catalyst for the selective Hydrogenation of cinnamaldehyde," *Journal of Chemistry*, vol. 2018, Article ID 5608243, 2018.

[16] X. Huang, L. Zhang, C. Li, L. Tan, and Z. Wei, "High selective electrochemical hydrogenation of cinnamaldehyde to cinnamyl alcohol on RuO2-SnO2-TiO2/Ti electrode," *American Chemical Society Catalysis*, vol. 9, no. 12, 2019.

[17] C. M. Cova, A. Zuliani, M. J. Muñoz-Batista, and R. Luque, "Efficient Ru-based scrap waste automotive converter catalysts for the continuous-flow selective hydrogenation of cinnamaldehyde," *Green Chemistry*, vol. 21, no. 17, 2019.

[18] Z. Konuspayeva, G. Berhault, P. Afanasiev, T.-S. Nguyen, S. Giorgio, and L. Piccolo, "Monitoring in situ the colloidal synthesis of $AuRh/TiO_2$ selective-hydrogenation nanocatalysts," *Journal of Materials Chemistry*, vol. 5, no. 33, 2017.

[19] F. Zhao, Y. Ikushima, M. Shirai, E. Takeo, and A. Masahiko, "Influence of electronic state and dispersion of platinum particles on the conversion and selectivity of hydrogenation of an α,β-unsaturated aldehyde in supercritical carbon dioxide," *Journal of Molecular Catalysis A: Chemical*, vol. 180, no. 1, pp. 259–265, 2002.

[20] Y. Li, H. Cheng, W. Lin et al., "Solvent effects on heterogeneous catalysis in the selective hydrogenation of cinnamaldehyde over a conventional Pd/C catalyst," *Catalysis Science and Technology*, vol. 8, no. 14, 2018.

[21] Z. Weng and F. Zaera, "Sub-monolayer control of mixed-oxide support composition in catalysts via atomic layer deposition: selective hydrogenation of cinnamaldehyde promoted by (SiO_2-ALD)-Pt/Al2O3," *American Chemical Society Catalysis*, vol. 8, no. 9, 2018.

[22] X. Ji, X. Niu, and B. Li, Q. Han, F. Yuan, F. Zaera, Y. Zhu, and H. Fu, Selective hydrogenation of cinnamaldehyde to cinnamal alcohol over platinum/graphene catalysts," *ChemCatChem*, vol. 6, no. 11, 2014.

[23] X. Z. Wei, X. Zhu, H. Liu et al., "Pt-Re/rGO bimetallic catalyst for highly selective hydrogenation of cinnamaldehyde to cinnamylalcohol," *Chinese Journal of Chemical Engineering*, vol. 27, no. 2, pp. 369–378, 2019.

[24] H. Pan, J. Li, J. Lu et al., "Selective hydrogenation of cinnamaldehyde with PtFe/Al2O3@SBA-15 catalyst: enhancement in activity and selectivity to unsaturated alcohol by Pt-FeO and Pt-Al2O3@SBA-15 interaction," *Journal of Catalysis*, vol. 354, pp. 24–36, 2017.

[25] S. Handjani, E. Marceau, J. Blanchard et al., "Influence of the support composition and acidity on the catalytic properties of mesoporous SBA-15, Al-SBA-15, and Al2O3-supported Pt catalysts for cinnamaldehyde hydrogenation," *Journal of Catalysis*, vol. 282, no. 1, pp. 228–236, 2011.

[26] S. S. Mohire and G. D. Yadav, "Selective synthesis of hydrocinnamaldehyde over bimetallic Ni-Cu nanocatalyst supported on graphene oxide," *Industrial & Engineering Chemistry Research*, vol. 57, no. 28, 2018.

[27] J. Hájek and D. Y. Murzin, "Liquid-phase hydrogenation of cinnamaldehyde over a Ru–Sn Sol–Gel catalyst. 1. Evaluation of mass transfer via a combined experimental/theoretical approach," *Industrial & Engineering Chemistry Research*, vol. 43, no. 9, 2004.

[28] G. Neri, L. Bonaccorsi, and S. Galvagno, "Kinetic analysis of cinnamaldehyde hydrogenation over alumina-supported ruthenium catalysts," *Industrial & Engineering Chemistry Research*, vol. 36, no. 9, 1997.

[29] H. Yamada, H. Urano, and S. Goto, "Selective hydrogenation of unsaturated aldehyde in gas-liquid-liquid-solid four phases," *Chemical Engineering Science*, vol. 54, no. 21, 1999.

[30] H. Liu, Z. Li, and Y. Li, "Chemoselective hydrogenation of cinnamaldehyde over a Pt-lewis acid collaborative catalyst under ambient conditions," *Industrial & Engineering Chemistry Research*, vol. 54, no. 5, 2015.

[31] O. S. Stamenković, V. B. Veljković, Z. B. Todorović, M. L. Lazić, I. B. Banković-Ilić, and D. U. Skala, "Modeling the

kinetics of calcium hydroxide catalyzed methanolysis of sunflower oil," *Bioresource Technology*, vol. 101, no. 12, 2010.

[32] M. L. Toebes, T. Alexander Nijhuis, J. Hájek et al., "Support effects in hydrogenation of cinnamaldehyde over carbon nanofiber-supported platinum catalysts: kinetic modeling," *Chemical Engineering Science*, vol. 60, no. 21, 2005.

[33] H. S. Fogler, *Elements of Chemical Reaction Engineering*, Pearson, London, UK, 2006.

[34] R. Ocampo-Pérez, J. Rivera-Utrilla, C. Gómez-Pacheco, M. Sánchez-Polo, and J. J. López-Peñalver, "Kinetic study of tetracycline adsorption on sludge-derived adsorbents in aqueous phase," *Chemical Engineering Journal*, vol. 213, pp. 88–96, 2012.

[35] G. Gandi, V. Silva, and A. Rodrigues, "Process Development for Dimethylacetal Synthesis: Thermodynamics and Reaction Kinetics," *Industrial & Engineering Chemistry Research*, vol. 44, 2005.

[36] J. Lee and D. H. Kim, "Global approximations of unsteady-state adsorption, diffusion, and reaction in a porous catalyst," *American Institute of Chemical Engineers*, vol. 59, no. 7, 2013.

[37] D. H. Kim, "A new linear approximation formula for cyclic adsorption in a biporous adsorbent," *Chemical Engineering Science*, vol. 52, no. 20, pp. 3471–3482, 1997.

[38] D. H. Kim and J. Lee, "High-order approximations for noncyclic and cyclic adsorption in a biporous adsorbent," *Korean Journal of Chemical Engineering*, vol. 16, no. 1, pp. 69–74, 1999.

[39] M. F. Friedrich, S. Kokolakis, M. Lucas, and P. Claus, "Measuring diffusion and solubility of slightly soluble gases in [CnMIM][NTf2] ionic liquids," *Journal of Chemical & Engineering Data*, vol. 61, no. 4, pp. 1616–1624, 2016.

[40] Y. Hou and R. E. Baltus, "Experimental measurement of the solubility and diffusivity of CO2 in room-temperature ionic liquids using a transient thin-liquid-film method," *Industrial & Engineering Chemistry Research*, vol. 46, no. 24, 2007.

[41] S. Pathak, A. Goswami, and S. Upadhyayula, "Kinetic modeling and simulation of catalyst pellet in the high temperature sulfuric acid decomposition section of Iodine-Sulfur process," *International Journal of Hydrogen Energy*, vol. 44, no. 59, 2019.

[42] P. Zámostný and Z. Belohlav, "A software for regression analysis of kinetic data," *Computers & Chemistry*, vol. 23, pp. 479–485, 1999.

[43] P. Virtanen, T. Salmi, and J.-P. Mikkola, "Kinetics of cinnamaldehyde hydrogenation by supported ionic liquid catalysts (SILCA)," *Industrial & Engineering Chemistry Research*, vol. 48, no. 23, 2009.

[44] Z. Shakor, A. AbdulRazak, and K. Sukkar, "A detailed reaction kinetic model of heavy naphtha reforming," *Arabian Journal for Science and Engineering*, vol. 45, 2020.

[45] Z. Shakor, M. J. Ramos, and A. A. AbdulRazak, "A detailed reaction kinetic model of light naphtha isomerization on Pt/zeolite Cctalyst," 2020, https://www.researchgate.net/publication/347524663_A_Detailed_Reaction_Kinetic_Model_of_Light_Naphtha_Isomerization_on_Ptzeolite_Catalyst.

[46] A. Al-Shathr, Z. M. Shakor, H. S. Majdi, A. A. AbdulRazak, and T. M. Albayati, "Comparison between artificial neural network and rigorous mathematical model in simulation of industrial heavy naphtha reforming process," *Catalysts*, vol. 11, no. 9, 2021.

[47] A. Hassanat, K. Almohammadi, E. A. Alkafaween, E. Abunawas, A. Hammouri, and V. B. S. Prasath, "Choosing mutation and crossover ratios for genetic algorithms-A review with a new dynamic approach," *Information*, vol. 10, no. 12, p. 390, 2019.